Radar tracking of synthetic particles in snow avalanches

Nico Haberstroh
Management Center
Innsbruck
Austria, 6020 Innsbruck
hn1260@mci4me.at

Anselm Köhler
Austrian Research Center for Forests (BFW)
Department of Natural Hazards
Austria, 6020 Innsbruck
anselm.koehler@bfw.gv.at

***Abstract*—In order to track particles within snow avalanches using high resolution radar, we develop and characterize an electronically amplifying radar reflector, known as an Active Target (AT). The AT, in conjunction with additional in-flow sensors, allows to analyze the flow dynamics of snow avalanches at the particle level. All measurements took place at the Nordkette mountain range above Innsbruck.**

The AT is analyzed and characterized including signal intensity changes with radar range. Initial tests for the moving AT scenario include roll measurements before the AT is directly placed in the avalanche. In addition to its primary function, the AT is used to calibrate the mGEODAR radar system itself by providing a known reference target to investigate ghost targets in the radar data due to internal hardware problems.

The study confirms the functionality of the newly developed Active target in combination with the radar device. However, the AT antenna's polarization and aperture require alignment of the AT with the radar beam. The signal intensity of the AT is at $40\,\mathrm{dB}$ for ranges larger than $200\,\mathrm{m}$ and for lower ranges, the target appears with increasing intensities that causes widening of the normally discrete target peak in the radar data. This is of minor importance for the avalanche measurements at typical distances between $300\,\mathrm{m}$ and $750\,\mathrm{m}$. Furthermore, those high intensity targets cause ghost targets at $207\,\mathrm{m}$ and $412\,\mathrm{m}$ in addition to the true target range. However, a comprehensive check of multiple radar settings does not reduce those mirror effects and the origin of the ghost targets can not be identified.

One successful avalanche event has been measured with the AT and the in-flow sensor system. The rolling and flowing of the AT causes the tracked trace to appear as recurring peaks in the radar data. Nevertheless, the trace enables direct synchronization between the in-flow particle data and the radar device, and thus resolves the particle location with respect to the snow avalanche.

July 31, 2024

I. Introduction

Avalanches especially snow avalanches are significant risks to human life, infrastructure and natural environments. It is crucial to understand dynamics and the flow behavior of snow avalanches to develop effective mitigation strategies and provide early warnings to infrastructure [1].

Multiple factors like the variety in snow type, mass grow due to entrainment and the terrain are responsible for the flow dynamics [2]. For deeper understanding of snow avalanches experimental and computational efforts are necessary.

Comprehending the dynamics of snow avalanches is essential for forecasting their destructive potential and movement. To achieve a detailed understanding of avalanche behavior at the particle level, an Active Target (AT) is developed to be tracked inside the flowing avalanche.

II. State of the art

Traditional methods of studying snow avalanches rely on observational data collected from remote sensoring, weather stations and visual surveys. Although these methods provide valuable insights, they often have limitations in accurately tracking individual snow particles within avalanche flow, particularly in complex terrains or during adverse weather conditions. Usage of synthetic particles in snow avalanches is one potential technological advancement in avalanche research and monitoring. Such in-flow sensors called AvaNodes were pioneered in the recent years at the BFW institute for natural hazards in Innsbruck [3].

Another method is the usage of radar technology which has revolutionized avalanche research by enabling precise and real-time tracking of avalanche flows. Radar systems can penetrate through snow layers and adverse weather conditions, providing continuous monitoring capabilities even in low visibility scenarios. By deploying radar systems strategically in avalanche-prone areas, researchers can gather detailed data on avalanche dynamics like flow velocities and runout distances.

The scientifically interesting radar devices are of frequency-modulated continuous wave (FMCW) radar technology [4]. This technology offers higher resolutions than detection radars. In contrast to detection radars, which are typically Doppler radars with a resolution of several meters, FMCW radars have submeter resolution and $0.37\,\mathrm{m}$ in the case of the herein used radar mGEODAR [5]. The mGEODAR performance is promising from laboratory tests, but the real world performance is still to be evaluated.

Providing a measurement tool for radar and target calibration itself and for tracking purposes inside avalanches an Active Target is developed in the further process.

A. Testsite Nordkette

The avalanche testsite Nordkette is reachable out of the city center Innsbruck. Therefore it is an ideal location for ongoing research into avalanche thematic. The measurements are carried out in the Seilbahnrinne where the radar device is

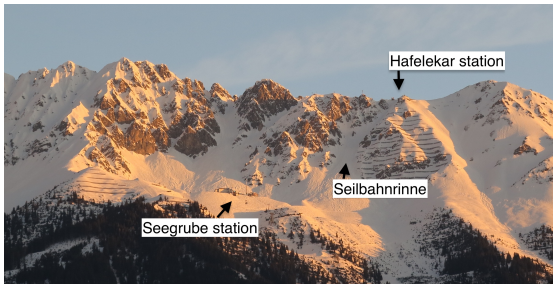

Fig. 1: Testsite of the Nordkette in the middle is the Seegruben station and right on top the Hafelekar station. The radar is located right next to the Seegrube station and points up to the Hafelekar station.

pointing upwards to the Hafelekar station. A gondola connects the Seegrube station with the Hafelekar station. A photo of the Nordkette is presented in figure 1. The gondola is important to mention because the radar measurements are affected by this gondola with unwanted reflections inside the radar data.

B. Radar system mGEODAR

The FMCW radar system mGEODAR has the following chirp signal configuration [6]:

TABLE I: FMCW radar configuration

Bandwidth B	$400\,\mathrm{MHz}$
Center carrier frequency f_0	$10.4\,\mathrm{GHz}$
Frequency band	$10.2\,\mathrm{GHz}$ to $10.6\,\mathrm{GHz}$
Chirp duration T	$10\,\mathrm{ms}$
Wavelength λ	$0.025\,\mathrm{m}$

Table I shows that each $10\,\mathrm{ms}$ chirp, corresponding to 100 chirps per second, is transmitted over the entire $400\,\mathrm{MHz}$ bandwidth, centered at $10.4\,\mathrm{GHz}$. The system operates within the $10.2\,\mathrm{GHz}$ to $10.6\,\mathrm{GHz}$ frequency band [5].

A simplified Blockdiagram of the FMCW radar system illustrates the minimal necessary components, including the receiver and transmitter chain with amplifier and antenna, in Figure 2.

Both chains are connected to mixers which combine the signals. Outgoing from the DDS chip (AD9914) which is clocked at $f_s = 3.48\,\mathrm{GHz}$ the Signal is produced and split. This chip generates a linear frequency ramp, called chirp. The chirp signal is up converted with a local oscillator (ADF5355) to reach the before mentioned frequency band of $10.2\,\mathrm{to}$ $10.6\,\mathrm{GHz}$. Further information about chirps can be found in following literature [4]. The power amplifier (AM31-10.2-10.7-37-37) with a gain of $37\,\mathrm{dB}$ strengthens the outgoing signal in the transmitter chain.

The modulated signal is transmitted and received through the antennas (SA15-90-104V-D1 from Cobham) with $15\,\mathrm{dB}$ gain [5]. Mixing the transmitted with the received signal yields a low frequency signal. This signal is recorded in the time domain with a single-channel 16-bit analog-to-digital converter at a maximum sample rate of $2\,\mathrm{MS/s}$ [7]. The stored raw data contains the target range r due to a relation between the chirp rate $\alpha = \frac{B}{T}$, the measured beat frequency

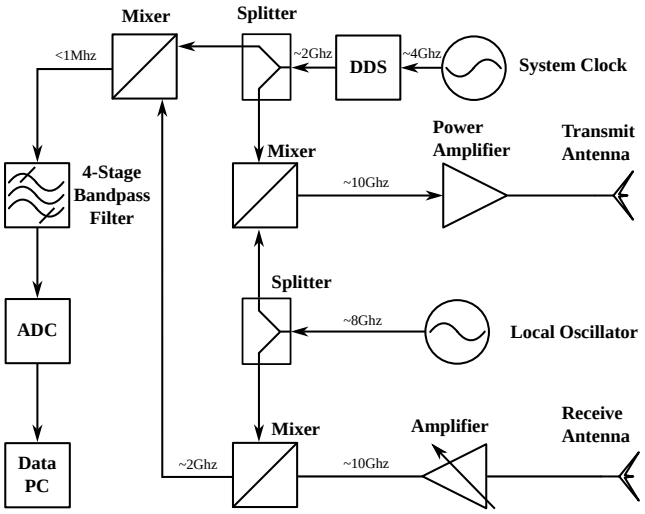

Fig. 2: Simple Blockdiagram of a FMCW radar system with signal processing and DDS chip [5].

f together with the signal propagation velocity c. Where B is the bandwidth and T the pulse duration in equation 1.

$$r = \frac{c * T}{2B} * f = \frac{c}{2\alpha} * f \tag{1}$$

The Doppler effect, a frequency shift due to target movement, appears additionally in the beat frequency f but is negligible in this system due to the short chirp duration and the expected avalanche velocities [8].

C. Active Target

An Active Target (AT) is a type of radar reflector that actively amplifies the incoming signal and transmits this signal back into the incoming direction.

Such an AT proved useful in the development of the predecessor radar GEODAR in the Swiss test-site Vallee de la Sionne [9]. Their AT is permanently installed in the middle of the avalanche track and represents a defined target throughout the whole winter seasons and is primarily used to ensure the radar operates properly. A second AT is in a mobile configuration and used for calibration purposes.

The components for an AT for the frequency range of the mGEODAR exist, but were only shortly used for quick tests during the radar development and initial avalanche measurements [10]. The results of these measurements were solely to prove the correct orientation of the radar antennas, but a complete characterization of the AT has never been done.

The Active Target (AT) is developed in the further process and consists out a receiver antenna (RX), transmitter antenna (TX), voltage supply, high-frequency amplifier and a status LED. It can be seen in photo 3.

III. Goal

The goal is to combine the methods of tracking synthetic particles inside avalanches with the help of radar observation.

Another objective is to investigate the capabilities of the radar system "mGEODAR" with the developed active target by providing a known reference target.

In a first step, an Active Target is developed and its performance is tested and characterized in the field using the mGEODAR radar as a signal source.

In a next step, the AT facilitates for calibration and validation of the radar system, and to minimize and optimize artifacts or inaccuracies inherent in the radar recordings. The focus is on two problems of the radar hardware. Firstly, the radar suffers from spectral leakage, so that targets may appear larger than they are. Secondly, mirror effects as sort of internal reflections cause ghost targets to appear in regular range intervals.

Lastly, the synthetic measurement particles AvaNodes are equipped with the AT. This AvaNode is then embedded onto the snowpack prior to an artificial avalanche release. The avalanche together with the particle is successfully tracked by the mGEODAR radar device. The particles should mimic the flow behavior of snow particles enabling to study avalanche dynamics. This paper contains selected results from an accompanying master thesis, where a more in depth investigation is found in [11].

IV. Methods

A. Concept of target development

The target comprises two antennas, one for receiving (RX) and one for transmitting (TX) with a high-frequency amplifier, serve as the heart of the target.

The first step is to figure out if the antennas are polarized and if so, in which direction it needs to be kept for successful measurements. Therefore different alignments of the antennas are investigated. The validation of the data results in following orientation of the antennas figure 3. It is important that the target is orientated in a precise way to obtain the wanted measurement results.

A battery-box for the power supply is needed for the voltage supply of the amplifier with the needed $5\,\mathrm{V}$ and $300\,\mathrm{mA}$, equals a power consumption of $1.5\,\mathrm{W}$. The function of the AT is, that the RX antenna receives the radar waves, and the signal passes through the amplifier, becoming stronger with a gain of $+20\,\mathrm{dB}$ before reaching the TX antenna to be returned. The signal then returns to the radar device, completing one cycle. Thus the target is identified with a strong peak in the radar data at the range from target to radar.

B. Data collection & Test-site

The measurements vary between calibration measurements, roll measurements and avalanche measurements. The calibration measurements are employed for the purposes of both calibrating the target and calibrating the radar. For this reason measurements with and without the AT were conducted. Prior to undertaking any measurements, it is necessary to ascertain that the radar is operational. This is achieved through the use of a telegram bot, which has been programmed by Anselm Köhler and interface implemented in Python. Consequently, it is possible to operate the radar remotely. The duration of calibration measurements is one second. In contrast, the roll and avalanche measurements are ranged from several minutes to one hour, depending on the completion time of the measurement. One hour of measurement contains about $30\,\mathrm{GB}$ of data which is a considerable amount for a remotely installed and autonomously running system.

It is important that the gondola, which ascends to the Hafelekar, is not within the operational area of the radar during measurements. Otherwise, there is a risk of introducing unwanted noise. In particular, this is relevant for the so-called zero measurement. A zero measurement is defined as a measurement conducted with no target or other moving objects in the line of sight of the radar.

C. mGEODAR radar & Data processing

In order to generate two-dimensional radar images of the recorded avalanches requires a number of signal processing steps which are detailed below. The existing Python processing codes convert radar data files into a format suitable for further postprocessing, including data cleaning and the application of filters and windows to enhance data quality [12].

First, the analog radar signal is rearranged into a two-dimensional dataframe using a marker signal to indicate active chirp pulses. In the current mGEODAR2 version, triggered acquisition stores the chirp raw data directly in this format. The key step in frequency-modulated continuous wave radar processing is the transformation from the time domain to the frequency domain via Fast Fourier Transformation (FFT). This transformation requires a window function to taper the signal to zero at the edges to prevent frequency sidelobes. A window with short cubic taper is used here, maintaining the middle $9\,\mathrm{ms}$ of the $10\,\mathrm{ms}$ chirp unchanged. The frequencies of the FFT are converted to range using equation 1 and the magnitudes of the FFT are calculated in decibels. For static measurements, or herein calibration measurements, the processing is finished, an example is shown in the upper panel of figure 4.

However, measurements of moving sceneries necessitate Moving Target Identification (MTI) filtering. The radar data includes reflections from various sources like rocks, dirt in the avalanche path or in case of the Seilbahnrinne the cablecar which create background clutter. MTI filtering compares chirps and subtracts amplitudes, removing stationary background clutter and displaying only moving targets. The applied MTI filter has 151 samples and a high-pass cut-off frequency of 0.12 reducing low frequencies changes from the static terrain. A following low-pass filter at a normalized frequency of 0.7 is also applied to remove high frequencies, that are related to electronic noise inside the radar.

Normalization in Moving Target Identification (MTI) is crucial. The mean intensity, calculated from periods when no movement is detected in the scene, serves as the normalization factor for each dataset. This process ensures smooth normalization curves and clean background levels.

MTI results, shown in figures 6, 8 and 9, display no movement with 0 dB intensities and moving targets with intensities up to 40 dB. MTI images are typically displayed in range time diagrams with slope of features correspond to line of sight velocity, i. e. velocity legend.

V. Realization

A. Design of the AT

The setup in figure 3 of the AT includes a voltage supply (5000 mAh which provides enough for 16 h measurement procedure), an amplifier, and two 10 GHz antennas where one is receiving and the other one transmitting. Additionally a GPS module has been placed next to the AT for determining the exact position. Therefore the distance between radar and the measuring position can be detected. For precise aligning the AT towards the radar device a scope and a spirit level is used. In order to ascertain the likelihood of the target being observed, the scope is employed to point directly on the radar. The status LED is employed for the purpose of verifying the sufficiency of the voltage supply. The shielding plate serves to ensure that the antennas are not subject to cross-coupling.

The intention of the design is to utilize the target in field measurements on a tripod setup, as well as to wrap around the concave cubic shape of the AvaNode for measurements inside the avalanche flow [3]. This means the cover needs to be rather durable to withstand the forces in an avalanche. Therefore, an organic mold was developed to minimize sharp edges that are prone to impacts. Out of this reason a 3D-printed case was designed [13]. This can be seen in figure 3. All the necessary items can be accommodated in this component and it can also be used as a field measuring instrument, offering a convenient solution. The figure 3 shows the developed target as a field measurement device.

Fig. 3: The assembled AT in the designed cover for protection

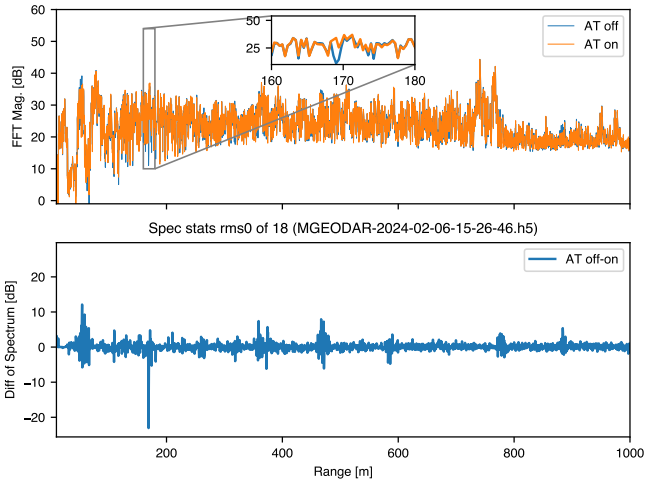

Fig. 4: Measurement with zoomed illustration of the AT position. Upper plot represents zero measurement in blue and target on in orange. The lower plot depicts the difference from target on subtracted from target off.

B. Experiment preparation & Execution

For calibration measurements the AT described is fixed on a tripod to locate it on the snow surface. Directly close to the Active Target is a GPS module situated to observe the exact position. With the aid of this it is possible to compare radar distance and the actual GPS position. With the aiming scope, the alignment of the AT can be carried out in order to align it directly in sight to the radar device.

The result of one measurement is presented in figure 4. The top plot illustrates the processed radar data with the AT activated (orange line) and off (blue line). The bottom plot shows the differences between the AT powered and AT not powered figure 4. The measurement time is one second.

The gray rectangle indicates the location of the AT. At approximately 169 m, the amplitude with the AT powered on is significantly higher compared to when it is powered off. This is evident in the zoomed section of the upper plot within the gray rectangle, highlighting a clear distinction between the on and off states. The difference plot also reveals a notable peak of -22 dB at this distance, confirming the position of the target.

Additional peaks in the difference plot may be attributed to various factors, including the gondola and its counterweight, human presence, but also ghost targets and multipath effects. The comparison between radar data and GPS data demonstrates that the radar range and GPS distance correspond at 169 m. The distance between the radar device and the GPS module at the AT's location is calculated using the haversine formula, which accurately determines distances between points on a sphere using latitude and longitude. Altitude is also incorporated into these measurements, calculated using the Pythagorean theorem.

The next measurement scenarios involve moving measurements, specifically roll and avalanche scenarios. For that

reason the AT and the AvaNode are encased in a cube-shaped foam in order to protect them from the effects of an avalanche. In the roll measurement, the AT was dislodged from a tripod at approximately $170\,\mathrm{m}$ to enable rolling towards the radar.

For the avalanche measurement at Nordkette, a minimum fresh snow depth of 20 cm was required. Upon confirmation, the Avalanche Commission initiated blasting operations. Data collection began with the blasting of the Seilbahnrinne area, releasing a cube containing the AvaNode and AT into the triggered avalanche. As the cube descended, the radar device collected data on avalanche speed, path, and length, providing valuable insights into avalanche behavior and characteristics.

VI. Results & Discussion

A. Calibration of AT

Calibration measurements showed that the AT antennas have an opening angle of $\pm 20^\circ$ in vertical as horizontal direction. Therefore the AT has a limited orientation where it is detectable for the radar. When the AT is oriented vertical towards the snow cover, multipath targets appear additional to the direct line of sight target [11]. The signal strength of the AT is sufficient to be tracked over all ranges, also because the baseband filter compensates geometric attenuation with range.

B. Mirror effects & ghost targets

Figure 5 shows 34 measurements between the Hafelekar (top) and Seegrube (bottom). Between each measurement are $20\,\mathrm{m}$ to $30\,\mathrm{m}$ distance. On the x-axis is the range from 0 to $1200\,\mathrm{m}$. The y-axis comprises difference plots from active target on and off, which have been normalized from 0 to 1. The uppermost plot corresponds to the target situated at $750\,\mathrm{m}$ range, which decreases to $150\,\mathrm{m}$ for the lowermost plot. The green line represents the direct path which can be connected through all the measurements. The line is not straight due to the non-equal spacing of the measurement points. Furthermore, it is evident in the data that there are ghost targets at distances of approximately $207\,\mathrm{m}$ and $412\,\mathrm{m}$ behind the direct signal of the true target. These are depicted in salmon and purple colors. In addition to the shifted ghost targets, there is a vertically reflecting mirror effect noticeable. This effect is visible in the lowest plot at around $300\,\mathrm{m}$ up to the eighth plot at around $190\,\mathrm{m}$ indicated by the orange line.

It is apparent that these mirror effects are not caused by multipath reflections because the ghost targets always occur at the same range offset from the true targets. Ghost targets due to antenna sidelobes or multiple reflections of snow and terrain surfaces would result in the same target appearing at random positions but can be excluded [14]. Therefore, these mirror effects are rather hardware-related problems inside the radar.

C. Radar settings

These mirror effects also cause in an avalanche measurement multiple ghost appearances in the radar data. Figure 6 represents the range-time MTI plot from the 25^{th} of January

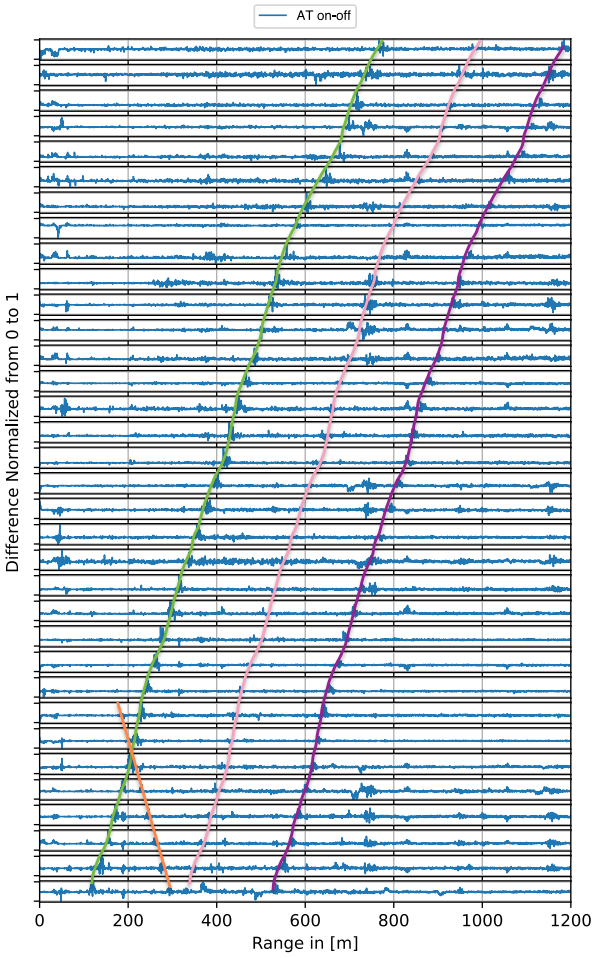

Fig. 5: Plot of static measurements in different ranges. The green line represents the true targets and the first and second ghost targets are indicated in salmon and purple, respectively. Vertically reflected ghost target at small ranges is shown with orange. Note: The green line is drawn along the true target while the other lines are copied and shifted to the ghost target positions.

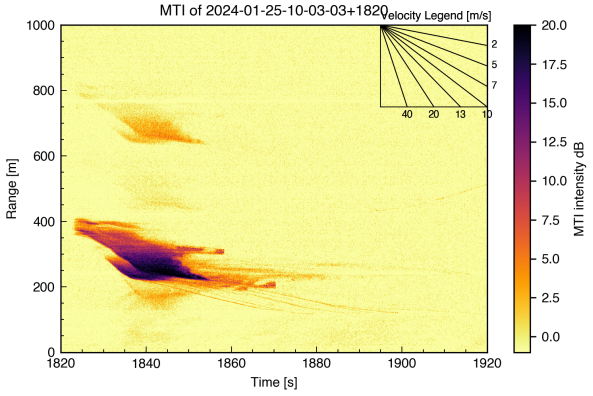

Fig. 6: Avalanche measurement from the 25.01.24 at 10:33 o'clock.

avalanche. It shows a very good example of this mirror effects in a measurement over time.

It is noteworthy that the avalanche descended from a distance of 400 to 160 m radar range. Small snowballs were observed emanating from the avalanche, visible as small orange stripes in the range of 200 to 100 m at a time between 1840 s to 1900 s. The intensity level of the avalanche is around 5 to more than 20 dB. Above the avalanche is the first ghost target detectable with very low signal starting at a range of 450 m and a time of around 1840 s. The second ghost target is more pronounced at a radar range of 800 to 650 m starting at around 1825 s. It is worthy to mention that this mirror effect only occurs when the intensity level of the target is above 15 dB which is herein called an over amplified target as discussed later in section VI-D. The first ghost target is slightly visible at a range of 207 m to the real target and the second at 412 m.

Accordingly, a number of radar settings are employed during data collection to mitigate the impact of mirror effects to suppress the ghost targets.

The analyzed settings can be divided in three groups:

- 4-stage baseband filter
- Receiver and transmitter chain
- Spurious signals

1) 4-stage baseband filter: Due to the over amplified targets above 20 dB, which can be observed in Figure 6, the objective of this measurement was to reduce the intensity level with the 4-stage active baseband filter to the point where a ghost target is no longer visible or the target is not over amplified anymore. The peak gain frequency is around 430 kHz or 1600 m range. Simulated response of the baseband filter for high and low gain response can be found in the mGEODAR hardware paper [5].

Upon examining the 4-stage baseband filter at its highest settings, it becomes evident that the majority of the signal is filtered out, resulting in a notable similarity between the noise and signal. Consequently, the Signal to Noise Ratio (SNR) is not a reliable indicator in this context. In contrast, other measurement points exhibit a significant difference between the signal from the Active Target (AT) and the noise. Thus, the AT is indistinguishable from different signals and the peak of the ghost target is obscured by the noise. With measurements midway through the baseband filter stages no serious changes to the default settings is noticed. It can be posited that modifying these settings is not the optimal approach for avoiding these mirror effects, because it reduces mainly the SNR values and for example weak avalanche signals will be lost with stronger baseband settings.

2) Receiver and transmitter chain: In the subsequent measurement process, the receiver and transmitter chain is altered. These measurements demonstrate minimal differences. If the transmitter chain's gain is insufficient, the difference between noise and the actual target becomes undetectable similar to the baseband settings section VI-C1. The disappearance of the ghost targets in a radar range of 207 m and 412 m is not achieved through changing amplifier or attenuator values in those chains. The Active Target is evident in every measurement scenario except the measurements where the transmitter chain gain was too low. Hence, even with modified signal strength, the desired elimination of the mirror effects remains unattained.

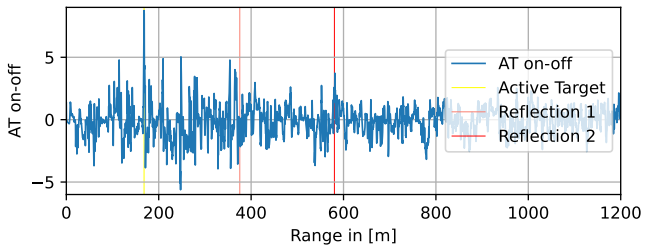

Fig. 7: Difference plot for measurement with changes in the DDS and Local Oscillator settings.

3) Spurious signals: These mirror effects give rise to a number of other reasons and namely the problem of spurious signals [15]. Many active high-frequency components are prone to have discrete noise spikes at discrete frequencies, mostly known as harmonics that are integer multiples of the operating frequency. However, those noise spikes can also occur at other frequencies and are commonly called spurious signals. These spurious signals, including harmonics, have always smaller signal intensities than the operating signal, the amplitude difference is the spurious free dynamic range.

The signal generation scheme for mGEODAR radar is composed of a DDS chip together with a local oscillator (LO) and with an up conversion mixer results in the desired transmit frequency 2. While the modification of the baseband and transmitter / receiver settings mainly focused on balancing the amplitude between the different frequency sections in the radar hardware, i.e. making optimal use of the spurious free dynamic range. The following paragraph tunes the DDS and the LO to a slightly different frequency region and therefor hoping to shift the spurious signal.

The default settings for the LO, the clock and DDS are 8.12 GHz, 3.48 GHz and a linear chirp from 2.08 GHz – 2.48 GHz, respectively. For the test to move the spurious signals, the settings for the LO, the clock and DDS are modified to 7.88 GHz, 3.7 GHz and the linear chirp from 2.32 GHz – 2.72 GHz, respectively. The idea was to change the high-frequency setting of every signal source, since every signal source can be the origin for spurious signals.

Figure 7 shows the difference-plot between a measurement with target off and target on for the full radar range. The main signal of the active target is a nearly 9 dB above the zero measurement. The second reflection is still visible at 580 m, but with 6 dB it is not the strongest spurious signal. Many more spurious signal appeared in between 200 m and 400 m, potentially, because the chirp data with these settings is not flat and unbalanced between lower and upper end of the chirp ramp.

In this case the signal distribution of the chirps occupies only one-third of the length compared to the relatively balanced chirp signal in the default settings. Unfortunately, the main outcome of this test settings is that the strong ghost target

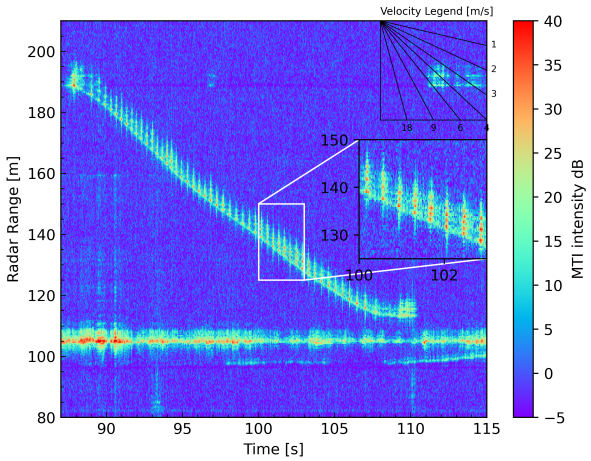

Fig. 8: Rolling target within the testside in a range from about 190 m to 120 m.

at +412 m does not disappear. So potential spurious signals of the frequency sources – DDS, clock and LO – are not the cause for the ghost targets and the origin of the mirror effects stays unclear.

D. Roll Measurement

The radar data of the roll measurement is shown in figure 8 with the range-time MTI plot. For the background normalization the first 8 s of the measurement are used. The rolling target are the diagonal recurring peaks from 190 m to 120 m range and between 87 s and 110 s. Also there are two ski touring individuals at a range of 100 m to 110 m who are moving slowly during the measurement over the full time span, and occasionally me moving slightly during the measurement at a range of 190 m are visible in the radar data. It is noticeable, that one ski touring person is reflecting with a high intensity of 25 to 40 dB at 110 m even though he remains stationary. This is due to the reason, that he is constantly in movement with his arms and is body. The second person is most of the time outside the viewing angle of the radar. He starts moving from 97 s till 105 s and constantly progresses into the radar field of view from 108 s onwards.

The active target exhibits high intensities of approximately up to 30 to 40 dB. In the zoomed inset at a distance of 125 m to 150 m and 100 to 103 s is the rolling AT depicted. Interestingly, the target appears with regularly spaced repeating peaks in intensity. The speed can be estimated to approximately $4\,\mathrm{m\,s^{-1}}$, which is derived from the velocity legend. The recurring peaks indicate the rotation of the target, as the orientation of the active target to the radar is very important, because of only one polarization and antenna aperture of 30° section VI-A. The peaks have an interval of approximately 0.4 s. This distance between the bottom of consecutive peaks is approximately four range bins which equals $4 * 0.37\,\mathrm{cm} = 1.48\,\mathrm{m}$. Taken the dimensions of the cube of 30 cm by 40 cm gives a total length of 1.4 m for a complete rotation.

It is evident that the peaks are distributed over several meters in range with multiple small intensity peaks, e.g. at 102 s are three small red peaks and for the next occurrence are five red peaks visible. The reason for this phenomenon remains unclear, but several possible effects can cause such spreading or widening of a single target. A first possibility can be due to the Doppler effect, as the range is influenced by velocity. However, the target exhibits a similar spread in the y-direction throughout the entire process, including the stationary phase from 108 s onwards. Therefore it is highly unlikely that the Doppler effect can be attributed here.

A second reason can be spectral leakage [16] during the processing of the radar data and the estimation of frequency, that relates to range in equation 1. Such spectral leakage can appear because of applying window functions which introduce sidelobes, or ripples, to the spectral density of the signal [17]. However, even when testing different window function prior to the FFT, the active target signal stays spread across multiple ranges.

Another explanation can be the multipath effect section VI-A. The prior found multipath targets are 2 m to 5 m larger than the true range. This is approximately the same distance at which the red intensity peaks in the highlighted area appear.

A more severe possible explanation for the spectral leakage can be internally in the radar hardware. Since the active target shows such high intensity about 30 to 40 dB, it is possible that certain components in the receiver chain are saturated which can cause a wide spread of the intensity over several frequencies and thus over several ranges. The high signal intensities can be therefore called over amplified intensities. The receiver chain consists basically of two mixers and some amplifiers to balance the signal levels. Due to the build of the radar on printed circuit boards, it is close to impossible to measure the signal in the receiver chain and therefore it is very difficult to rule out this possible explanation. Needless to say, the active target is a good method to identify such problems, and future repeats of these measurements could involve changing internal radar parameters as it has been done in the laboratory in [5].

E. Avalanche Measurement with Active Target

The plot 9 shows an avalanche measurement, recorded on the 20.02.24 with the AT and an AvaNode in-flow sensor inside the avalanche. The occurrence of the avalanche is clearly visible in the center of the plot, resulting from a change in intensity due to the MTI filtering. The orange coloration indicates a heightened intensity, which is a consequence of the moving avalanche in the radar data. The avalanche started at a radar range from about 750 m and descended to approximately 300 m in a time window of 50 s. The ghost target in a range of 412 m is also visible at a timestamp of 2340 s to 2365 s. Inside this avalanche the AT is recognizable at the upper part of the avalanche in the region of 750 m to 650 m.

The GPS data of the AvaNode clearly demonstrates that the AT follows the path of the avalanche and even has the same speed as the avalanche itself. In the initial section extending from 750 m to 650 m the velocity of the cube and avalanche amounts to $4\,\mathrm{m\,s^{-1}}$. Subsequently the velocity increases to

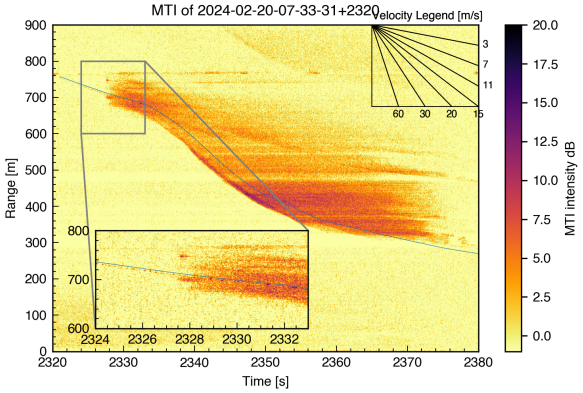

Fig. 9: Avalanche measurement with Active Target and GPS validation at the 20.02.24

approximately $15\,\mathrm{m\,s^{-1}}$ until $500\,\mathrm{m}$. From there on both entities exhibit a deceleration, reaching a velocity of around $4\,\mathrm{m\,s^{-1}}$. The avalanche remains at a distance of $300\,\mathrm{m}$ after nearly $50\,\mathrm{s}$ while the measurement cube continuous to roll down.

It is immediately apparent from the zoomed inset that there are again the repeated peaks in intensity which are known from the roll measurements figure 8 from $730\,\mathrm{m}$ to $680\,\mathrm{m}$. These peaks are representing the AT.

It is perceptible that the radar data and the GPS data has a small offset. This offset comes of a time offset. The time in the GPS is recorded in one second steps which leads to small uncertainties. Furthermore the GPS data is not atmospheric corrected which causes a systematic error. This means that the location accuracy is limited to 3 to $5\,\mathrm{m}$.

After $680\,\mathrm{m}$ the active target is not visible anymore. The reason for that could be that the cube is under a too thick layer of snow, the power supply has an interruption or the antenna cable became loose due to the avalanche motion. Nevertheless the target is visible in the beginning and the in-flow sensor can be directly synchronized with the radar data which previously had to rely on simultaneous clocks [3]. Consequently the trajectory of the synthetic particle can be traced with great precision and with the reference of the overall avalanche that the radar image provides.

VII. Conclusion

The objective of this paper includes the development and tracking of the AT in an avalanche scenario and using this AT in various measurement scenarios, such as calibration, roll and avalanche measurements to improve the mGEODAR radar performance.

The development and functionality of the AT, along with its calibration using the mGEODAR radar, are successfully accomplished. The AT operates effectively for all relevant ranges, when oriented within $\pm 20^\circ$ along the line of sight of the radar.

Existing avalanche measurements reveal mirror effects in the radar hardware that cause ghost targets to appear at consistent range offsets and are investigated through calibration measurements. Multiple radar settings are tested to vary the baseband filter, the receiver and transmitter chain as well as the high-frequency signals sources. Although problematic ghost targets persist as shown in figure 6, they only occur when targets are over amplified, typically within $300\,\mathrm{m}$ of the radar range. These over amplified targets additionally exhibit spectral leakage, causing their detected location to spread over several meters.

The combination of radar technology with the AT and an in-flow sensor acting as a synthetic particle proves effective. It is possible to track the AT inside an avalanche enabling synchronization between in-flow sensor data and radar data.

Using an AT with a radar device represents a significant advancement, providing a known reference target for field measurements and simplifying the use of complex radar devices. Despite these advances, challenges remain. Multipath effects, environmental factors, snowpack variability, and hardware issues can hinder measurement accuracy. Careful calibration and ongoing adjustments are necessary and an AT is an ideal tool.

In conclusion, the gained insights from roll and avalanche measurements, the calibration of the radar system by applying various radar settings have improved the understanding of the radar device mGEODAR. Further improvements of the AT include shape adjustments or the use of omnidirectional antennas. Future research should continue exploring these technologies to enhance precision and applicability in other tracking applications.

Acknowledgment

This project has been financed by the Unit of Snow and Avalanches (BFW) Innsbruck.

References

[1] J. Schweizer, J. B. Jamieson, and M. Schneebeli, “Snow avalanche formation,” *Reviews of Geophysics*, vol. 41, no. 4, 2003. doi: 10.1029/2002RG000123

[2] T. Faug, B. Turnbull, and P. Gauer, “Looking beyond the powder/dense flow avalanche dichotomy,” *Journal of Geophysical Research: Earth Surface*, vol. 123, no. 6, pp. 1183–1186, 2018. doi: 10.1002/2018JF004665

[3] M. Neuhauser, A. Köhler, R. Neurauter, M. S. Adams and J.-T. Fischer, “Particle trajectories, velocities, accelerations and rotation rates in snow avalanches,” *Annals of Glaciology (IGS)*, 2023. doi: 10.1017/aog.2023.69

[4] M. J. Ash, P. V. Brennan, C. J. Keylock, N. M. Vriend, J. N. McElwaine, B. Sovilla, “Two-dimensional radar imaging of flowing avalanches,” *Cold Regions Science and Technology*, 2013.

[5] A. Köhler, L. B. Lok, S. Felbermayr, N. Peters , P. V. Brennan , and J.-T. Fischer, “mGEODAR – a mobile radar system for detection and monitoring of gravitational mass-movements,” *Sensors*, October 30, 2020.

[6] S. Felbermayr, “Scheckkartencomputer-basierte Datenerfassung für ein mobiles Lawinenradar,” Bachelor Thesis, Management Center Innsbruck, 2020.

[7] J.-J. Lin, Y.-P. Li, W.-C. Hsu, and T.-S. Lee, “Design of an FMCW radar baseband signal processing system for automotive application,” *SpringerPlus*, vol. 5, no. 1, p. 42, 2016. doi: 10.1186/s40064-015-1583-5

[8] Z. Zahra, “Stimulation eines Radar-Objekterkennungs- und Trackingverfahren mit synthetischen Daten,” Master Thesis, Technische Universität Darmstadt, 2020.

[9] A. Köhler, "High resolution radar imaging of snow avalanches," Dissertation, Durham University, 2017. [Online]. Available: http://etheses.dur.ac.uk/12556/
[10] M. Winkler, "Vergleich von AvaFrame-Lawinensimulationen mit mGeodar-Radarmessungen am Beispiel von gesprengten Lawinen auf der Nordkette," Master Thesis, Universität Innsbruck, 2022.
[11] N. Haberstroh, "Radartracking of synthetic particles in snow avalanches," Master Thesis, Management Center Innsbruck, 2024.
[12] A. Köhler, "Code repository," Accessed: 15.02.24. [Online]. Available: https://bitbucket.org/snowavalanche/fmcw_processing/src/master/
[13] N. Haberstroh and A. Köhler, "3D print design for mgeodar active target cover," *Zenodo*, 2024. doi: 10.5281/zenodo.12801962
[14] G. E. Smith and B. G. Mobasseri, "Multipath exploitation for radar target classification," in *2012 IEEE Radar Conference*, 2012. doi: 10.1109/RADAR.2012.6212215 pp. 0623–0628.
[15] A. W. Doerry, D. L. Bickel, "Discriminating spurious signals in radar data using multiple channels," *Sandia National Laboratories*, 2012.
[16] N. Tomen, J. C. v. Gemert, "Spectral Leakage and Rethinking the Kernel Size in CNNs," *Computer Vision Lab, Delft University of Technology*, 2021.
[17] S. W. Smith, *The Scientist and Engineer's Guide to Digital Signal Processing*, 2nd ed. California Technical Publishing San Diego, California, 1999.